SANDIA REPORT
SAND2021-0865
Printed January 2021

Sandia National Laboratories

Modeling Framework for Bulk Electric Grid Impacts from HEMP E1 and E3 Effects

EMP-Resilient Grid Grand Challenge: Task 3.1 Final Report

Brian Pierre, Daniel Krofcheck, Matthew Hoffman, Ross Guttromson, Richard Schiek, Jimmy Quiroz

Prepared by
Sandia National Laboratories
Albuquerque, New Mexico
87185 and Livermore,
California 94550

Issued by Sandia National Laboratories, operated for the United States Department of Energy by National Technology & Engineering Solutions of Sandia, LLC.

Available to DOE and DOE contractors from
U.S. Department of Energy
Office of Scientific and Technical Information
P.O. Box 62
Oak Ridge, TN 37831

Telephone: (865) 576-8401
Facsimile: (865) 576-5728
E-Mail: reports@osti.gov
Online ordering: http://www.osti.gov/scitech

Available to the public from
U.S. Department of Commerce
National Technical Information Service
5301 Shawnee Rd
Alexandria, VA 22312

Telephone: (800) 553-6847
Facsimile: (703) 605-6900
E-Mail: orders@ntis.gov
Online order: https://classic.ntis.gov/help/order-methods/

ABSTRACT

This report presents a framework to evaluate the impact of a high-altitude electromagnetic pulse (HEMP) event on a bulk electric power grid. This report limits itself to modeling the impact of EMP E1 and E3 components. The co-simulation of E1 and E3 is presented in detail, and the focus of the paper is on the framework rather than actual results. This approach is highly conservative as E1 and E3 are not maximized with the same event characteristics and may only slightly overlap. The actual results shown in this report are based on a synthetic grid with synthetic data and a limited exemplary EMP model. The framework presented can be leveraged and used to analyze the impact of other threat scenarios, both manmade and natural disasters.

This report describes a Monte-Carlo based methodology to probabilistically quantify the transient response of the power grid to a HEMP event. The approach uses multiple fundamental steps to characterize the system response to HEMP events, focused on the E1 and E3 components of the event.

1) Obtain component failure data related to HEMP events – testing of components and creating component failure models. Use the component failure model to create component failure conditional probability density function (PDF) that is a function of the HEMP induced terminal voltage.

2) Model HEMP scenarios and calculate the E1 coupled voltage profiles seen by all system components. Model the same HEMP scenarios and calculate the transformer reactive power consumption profiles due to E3.

3) Sample each component failure PDF to determine which grid components will fail, due to the E1 voltage spike, for each scenario.

4) Perform dynamic simulations that incorporate the predicted component failures from E1 and reactive power consumption at each transformer affected by E3. These simulations allow for secondary transients to affect the relays/protection remaining in service which can lead to cascading outages.

5) Identify the locations and amount of load lost for each scenario through grid dynamic simulation. This can be an indication of the immediate grid impacts from a HEMP event. In addition, perform more detailed analysis to determine critical nodes and system trends.

6) To help realize the longer-term impacts, a security constrained alternating current optimal power flow (ACOPF) is run to maximize critical load served.

This report describes a modeling framework to assess the systemic grid impacts due to a HEMP event. This stochastic simulation framework generates a large amount of data for each Monte Carlo replication, including HEMP location and characteristics, relay and component failures, E3 GIC profiles, cascading dynamics including voltage and frequency over time, and final system state. This data can then be analyzed to identify trends, e.g., unique system behavior modes or critical components whose failure is more likely to cause serious systemic effects. The proposed analysis process is demonstrated on a representative system. In order to draw realistic conclusions of the impact of a HEMP event on the grid, a significant amount of work remains with respect to modeling the impact on various grid components.

ACKNOWLEDGEMENTS

Supported by the Laboratory Directed Research and Development program at Sandia National Laboratories, a multimission laboratory managed and operated by National Technology and Engineering Solutions of Sandia LLC, a wholly owned subsidiary of Honeywell International Inc. for the U.S. Department of Energy's National Nuclear Security Administration under contract DE-NA0003525.

CONTENTS

1. Introduction 9
2. HEMP Model and Coupling Analysis 12
3. Component Testing and Failure Modes 16
4. Electromechanical Dynamic Transient Simulations While Including Cascading Failures 18
   4.1. The IEEE Reliability Test System (RTS-96) Modifications 18
   4.2. Modeling HEMP E3 20
      4.2.1. RTS-96 E3 Impact Locations 20
      4.2.2. E3 GIC Calculations 21
      4.2.3. Reactive Power Loss Simulation 22
   4.3. Modeling HEMP E1 with E3 23
5. Analysis Framework – Critical nodes, states, and transitions 25
   5.1. Data Processing and Preparation 25
   5.2. Synoptic Load Shed and Scenario Failure Distributions 26
   5.3. Critical System States and Transitions 29
   5.4. Implications for High Component Failure Scenarios 32
   5.5. Sources of Cascading Uncertainty 35
6. Conclusions 37

Appendix A – Deep Learning for Network Topology Similarity 40

LIST OF FIGURES

Figure 1-1. Overall architecture of Sandia's EMP project with an aim to achieve a grid more resilient to EMP events: 1) understand EMP consequences to grid components, 2) develop new materials and components to mitigate component damage from EMP events, 3) identify electric power grid systemic response to EMP events. 9
Figure 1-2. The overall EMP grid consequence analysis flow chart 11
Figure 2-1. Scaling field for E0 used in E1 calculations 13
Figure 2-2. Two simulation examples of the E1 EMP induced voltage seen by a relay in an IEEE test system. 14
Figure 2-3. Histogram of E1 EMP induced max voltage levels at all the relays in an IEEE test system for 1000 synthetic HEMP scenarios. 15
Figure 3-1. Relay failure sampling curve. Area 1 is the relay failed, but only needed a power cycle to continue to operate. Area 2 is the relay fully failed (permanently damaged). Area 3 is the relay operated normally. For Monte Carlo sampling, give a voltage level (e.g. 80 kV), a random number between 0 and 1 is selected (e.g. 0.5), and the relay reaction is dependent on where that point falls in the figure (e.g. 80,0.5 falls in Area 2, so the relay is permanently damaged). Derived from data in [22]. 17
Figure 4-1. The power system co-simulation of EMP E1 and E3 methodology 18
Figure 4-2. The RTS-96 Three Area system diagram [23] with reactive power burden locations highlighted in yellow. 21
Figure 4-3. EMP E3 GIC current values at all 51 buses in the RTS-96 system for one synthetic HEMP scenario. 22
Figure 4-4. E3 impact incorporation overview 22

Figure 4-5. The voltage degradation due to EMP E3 transformer saturation at a set of buses in the RTS-96 system, for an exemplary HEMP scenario. Note, this is a result while considering E3 only impacts, and has many other assumptions built in.....23
Figure 5-1. Number of failures for generators in the RTS-96 system through time, for the 1000 E1 + E3 scenarios sampled. Lighter colors indicate more component failures. Each plot describes the likelihood of failure of generators for each subgrid A, B, and C. Note the Y-axis is non-linear, ranging from PSLF simulation start (top) to finish (bottom).....27
Figure 5-2. Number of failures for lines in the RTS-96 system through time, for the 1000 E1 + E3 scenarios. Lighter colors indicate more component failures. Each plot describes the likelihood of failure of lines for each subgrid A, B, and C. Note the Y-axis is non-linear, ranging from PSLF simulation start (top) to finish (bottom).....28
Figure A-1. Deep learning diagram [24]. 40

LIST OF TABLES

Table 4-1. Generator Under/Over Frequency Tripping 19
Table 4-2. Generator Under/Over Voltage Tripping 19
Table 4-3. Under Frequency Load Shedding Schedule 19

This page left blank

ACRONYMS AND DEFINITIONS

Abbreviation	Definition
ACOPF	Alternating Current Optimal Power Flow
CT	Current Transformer
DCOPF	Direct Current Optimal Power Flow
EMP	Electromagnetic Pulse
GED	Graph Edit Distance
HEMP	High Altitude Electromagnetic Pulse
IEEE	Institute of Electrical and Electronic Engineers
PDF	Probability Density Function
PT	Potential Transformer
RTS-96	Reliability Test System from 1996

1. INTRODUCTION

A high-altitude electromagnetic pulse (HEMP) event is an artifact of a nuclear explosion kilometers above Earth's surface. Such explosions can be designed to minimize mechanical damage while maximizing electromagnetic pulses, which can wreak havoc in electrical and electronic gear [1], [2]. Some facilities have been designed to withstand electromagnetic pulse (EMP) events, including many grid control centers.

Sandia National Laboratories has initiated a multi-year investigation that is summarized in Figure 1-1 [3]. The first part is focused on achieving a better understanding of the consequences to grid components, for example: transformers, relays, SCADA systems, potential transformers (PTs), current transformers (CTs), breaker control circuitry, photovoltaics, inverters, and more due to HEMP exposure. The second part focuses on the development of new materials to mitigate or prevent damage resulting from the systemic effects of a HEMP event. The third part, which is the focus of this report, works to develop a framework to estimate the electric power grid response to a HEMP event.

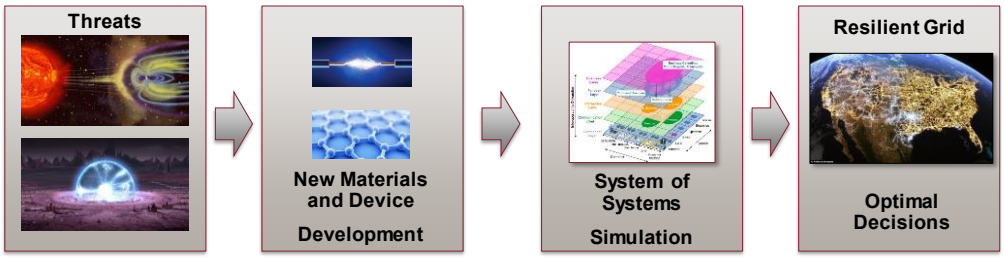

Figure 1-1. Overall architecture of Sandia's EMP project with an aim to achieve a grid more resilient to EMP events: 1) understand EMP consequences to grid components, 2) develop new materials and components to mitigate component damage from EMP events, 3) identify electric power grid systemic response to EMP events.

An EMP event is typically broken down into three phases [4]. Phase E1 [5], peaking at about 50kV/m after approximately 2.56ns and has decayed to near zero before 0.1μs [6]. Phase E2, peaking at about 100V/m, extends to several milliseconds [6]. Phase E3, less than 100mV/m, extends to hundreds of seconds [6] and appears very much like a geo-magnetic disturbance (GMD) [7], [8]. We must consider E1, E2, and E3 in this grid analysis framework. Note that E2 is often considered to be similar to lightning and will be a topic for future work. E3 is often considered to be similar to GMD. In this report we co-simulate the grid impacts from E1 and E3.

This report summarizes the framework to analyze the electric power grid response to HEMP events. This report will focus on the overall framework rather than specific results. An overview of the modeling approach is summarized in Figure 1-2. The approach uses a dynamic bulk electric power system positive sequence model that covers a large geographical area and the high voltage transmission system. In addition, a detailed protection model needs to be integrated with the positive sequence model to allow secondary transients and cascading failures. The framework can be broken into steps:

1. The first step is to develop component level failure models. These models are based on component testing and analysis. Sandia testing involves conducted pulse testing to represent the E1 event [9], and examples of Sandia component testing are in [9] – [12]. The component level model provides information on the probability of different failure modes given an induced terminal voltage. For example, for a relay, there are two different failure modes: fail closed (no change in contact position, but no longer functions as a relay) and fail open (change in contact position and no longer functions as a relay). There is also fail temporary (where a power cycle will

allow the relay to continue operation) and fail permanent (permanent physical damage and in need of repair or replacement). Therefore, the component failure model is given as:

$$p(fail|induced\ terminal\ voltage) = f_1(terminal\ voltage)$$
$$p(fail\ open|fail) = f_2(terminal\ voltage)$$
$$p(fail\ closed|fail) = 1 - p(fail\ open|fail)$$
$$p(fail\ temporay|fail) = f_3(terminal\ voltage)$$
$$p(fail\ permanent|fail) = 1 - p(fail\ temporay|fail)$$

2. Create and model HEMP scenarios. Given thousands of HEMP possibilities (latitude, longitude, altitude, strength, etc.), create scenarios for each HEMP event. Every scenario includes the induced voltage profile seen at the terminal of each grid component in the bulk electric system model.
3. Based on the HEMP induced voltage profile at each grid component, and the component failure models, sample each HEMP scenario to create grid failure scenarios (i.e. which grid components are removed from service due to the HEMP event). In addition, sample a time of failure PDF. Although an EMP E1 wave is complete within a microsecond, the propagation of the failure to the actual removal of a transmission grid component may take more time.
4. Perform dynamic simulations that incorporate the predicted component failures. These simulations allow for secondary transients, which can trigger protection relays remaining in service, which can lead to cascading outages.
5. Employ dynamic simulations to quantify the impact of each EMP scenario. Metrics include location of lost load, amount of lost load, component failures, and grid collapse. The electromechanical transient dynamic simulations can be used to identify the immediate grid impacts from a HEMP event. In the dynamic simulation, the HEMP event damages components or causes component mis-operation causing grid components to be removed from service, such as generators, transformers, transmission lines, or loads (entire feeders or sections of a distribution system). The remaining protection system reacts to transients caused by component trips, this protection system can then trip more components leading to cascading failures.
6. To help realize the longer-term impacts, a security constrained AC optimal power flow (ACOPF), or DCOPF is run to maximize critical load served. The security constrained OPF enables all components that were removed from service due to secondary transients, but the components that were physically damaged from the EMP event remain out of service and need repair or replacement. The load that cannot be served after an OPF signifies the longer-term impacts from the EMP event, and that load will remain unserved until components are repaired or replaced.

Finally, the entire analysis framework is applied to a representative system to illustrate the process for evaluating E1+E3 grid impacts. The results can indicate trends, critical components, failure clusters, cascading failure flow diagrams, and more.

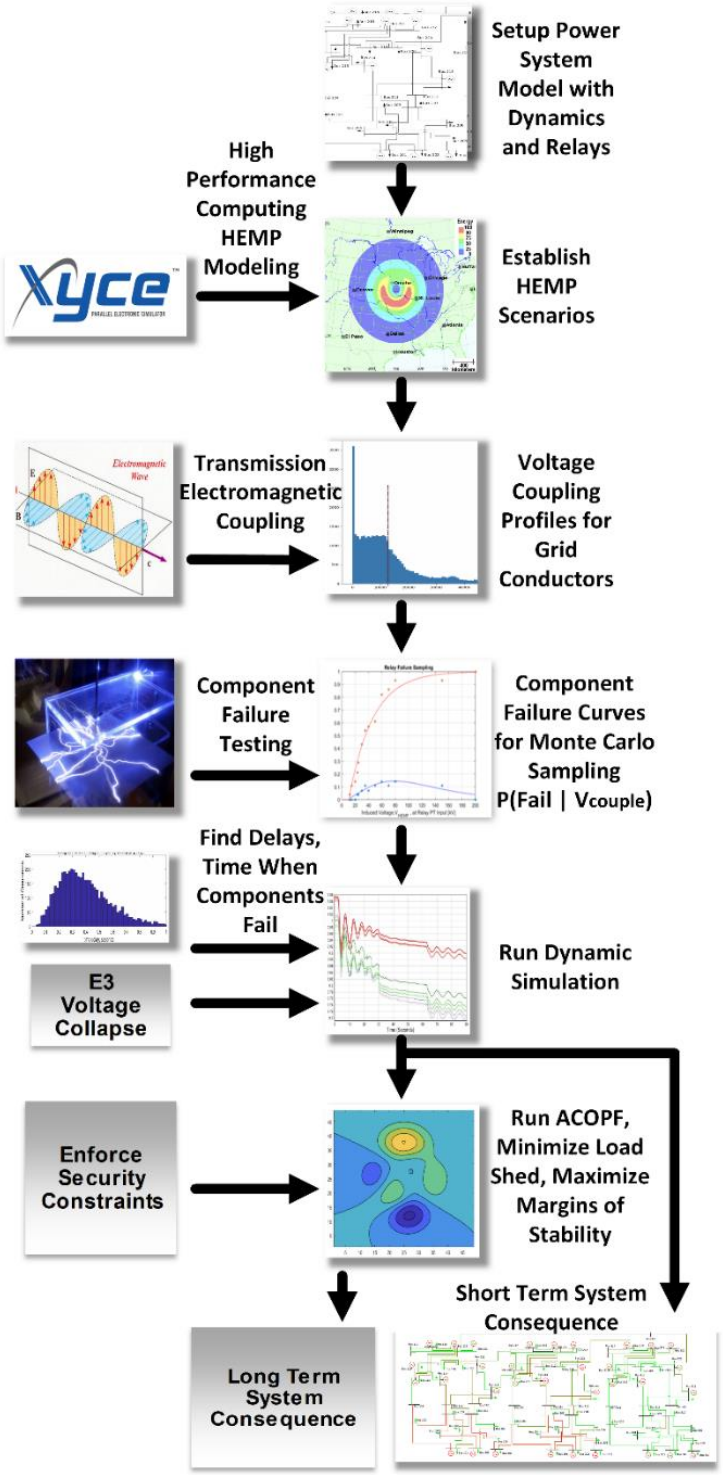

Figure 1-2. The overall EMP grid consequence analysis flow chart

2. HEMP MODEL AND COUPLING ANALYSIS

The component failures depend on the EMP induced voltage at the component's input terminals (and may also depend on induced voltages within the device itself). There is significant research on the induced voltages caused by HEMP events [13]. For each scenario, the HEMP model calculates the coupled voltage, which is an input to the component failure model; p(fail | induced terminal voltage). Each failure model is then sampled to determine if that component fails for that scenario. Once a component is deemed to have failed, the component is removed during a power system dynamic simulation, and/or if the failed component causes other components to trip offline, then those components are also disabled during a dynamic simulation.

The HEMP model is based on the work described in [14]-[16]. The HEMP model calculates an irradiated field and then performs coupling analysis to determine the coupled voltage. The voltage imposed upon each component by the HEMP event is dependent on:

1. the HEMP magnitude and model type (IEC HEMP standard used for E1 and explained below).
2. the HEMP geographic location and direction (altitude, latitude, longitude with respect to each line and component on the grid)
3. the length and size of the line or cable,
4. the orientation of the conductor coupling the transverse electromagnetic (TEM) wave with respect to the HEMP's E-field polarization,
5. the conductor coupling the TEM wave's termination impedance for frequencies up to 100MHz.

Some of these parameters (such as HEMP location) are inherently uncertain, and varied scenarios can be developed by sampling over reasonable distributions for these parameters. In each scenario, the HEMP location and size changes, all other parameters stay constant. Each HEMP scenario results in a coupled voltage profile at every component in the system.

The HEMP source used for this work is the IEC HEMP Standard [17]. The E1 environment used requires that the maximum magnitude of the pulse (E0) is scaled according to the location of the observer on the surface of the earth relative to the blast. The contours of this scaling field are shown in Figure 2-1. Thus, based on a location of the RTS-96 system relative to the HEMP event, the E0 used in the simulation is scaled appropriately to comply with the intended constraints of the IEC HEMP standard (see Figure 6 of [17] for a comparative example). Prior to scaling, E_0=50,000 V/m and a_1=4e7 s^{-1}, b_1= 6e8 s^{-1}, k_1=1.0.

$$E_1 = E_0 k_1 (e^{-a_1 t} - e^{-b_1 t})$$

In this double-exponential formulation, E_0 represents a maximum magnitude of the pulse and k_1 is a scaler used to modify the magnitude for local conditions. In this work one can consider the contour plot of Figure 2-1 as a spatial function for k_1. The constants a_1 and b_1 control the growth and decay of the overall waveform respectively.

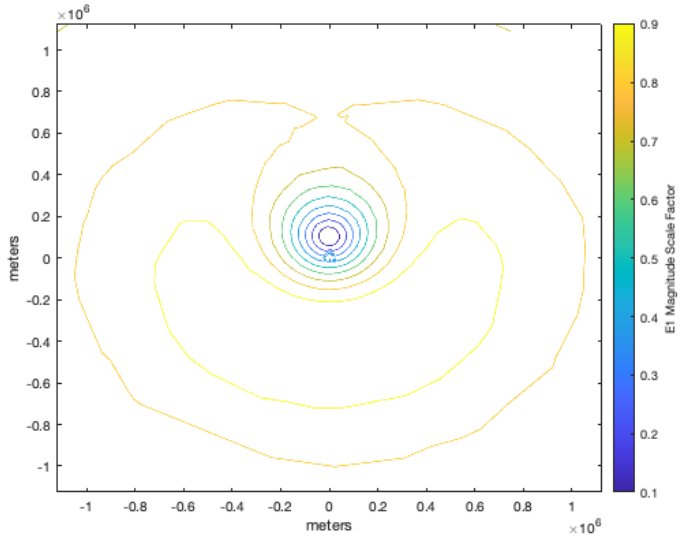

Figure 2-1. Scaling field for E0 used in E1 calculations

The E3 environment used is as described in the IEC HEMP standard with the following parameters used for this work:

E_{i0} = 0.04 V/m, k_i = 1.058, a_i=0.02 s^{-1}, b_i=2.0 s^{-1}, τ =t-1

$$E_i = E_{i0}\, k_i\, (e^{-a_i\tau} - e^{-b_i\tau})$$

E_{j0} = 0.01326 V/m, k_j = 9.481, a_j=0.015 s^{-1}, b_j=0.02 s^{-1}, τ =t-1

$$E_j = E_{j0} k_j \left(e^{-a_j\tau} - e^{-b_j\tau}\right)$$

$$E_3 = \left(E_i - E_j\right)$$

Like E1, the E3 formulation is based on a double-exponential, but with two sets of growth and decay terms (for a total of four exponentials). As with E1, the E_{i0} and E_{j0} terms control the maxima of the early and late E3 waveform respectively. The a_i, b_i are time scales for the early E3 and a_j and b_j time scales for the late E3. Both k_i and k_j are scalers used for local adjustment of the maxima. They were fixed at the values shown for all simulations in this work.

The electrical circuit simulator Xyce [18] is used to perform the coupling analysis to generate the device voltage profiles. Xyce is a Spice style electrical circuit simulator that solves for currents and voltages on a circuit network through the application of device equations and Kirkoff's voltage and current laws. In all cases an equivalent electrical circuit for the transmission line and connected equipment is constructed and then connected to the EMP environment as in [14]-[15]. This is effectively Telegrapher's equations with additional terms for the external EMP field,

$$L\frac{\partial I}{\partial t} + R\, I = V_{HEMP} - \frac{\partial V}{\partial z}$$
$$C\frac{\partial V}{\partial t} + G\, V = -\frac{\partial I}{\partial z}$$

where L, C, R, and G are inductance, capacitance, resistance and conductance for the conductor line on per unit length basis. Z is the coordinate along the transmission line and V and I are the voltage and current through a given segment of the line and V_{HEMP} is the locally induced voltage on a line segment due to the EMP field. Accurately modeling the HEMP voltage coupling is much more complicated than this brief explanation, and refs. [19] and [20] include more details (that go beyond Telegrapher's equations) on Sandia's Xyce modeling of HEMP voltage coupling.

Each HEMP event results in an E1 coupled voltage profile similar to Figure 2-2 for each component. In this work E1 is coupled into the sensor lines at the substations of the synthetic grid system. Figure 2-2 is an example of the coupling voltage on a cable from a potential transformer (PT) to a relay. For our analysis, the maximum voltage is an input to each component's failure model. A histogram of the maximum voltage seen by relays throughout the synthetic test system from coupling on the cable between the PT and the relay is seen in Figure 2-3 (note this is developed with synthetic data). Similar data is gathered for coupling on transmission lines and cables throughout a test system. And similar data to Figure 2-3 is developed for the maximum coupling voltage levels seen at all components in the system.

In addition to E1 coupling voltage profiles, similar profiles (over a much longer timeframe) are created for E3. The primary goal of modeling E3 has focused on the saturation of transformers and their corresponding consumption of reactive power; this may cause significant voltage issues in the system. Thus, for E3, the coupling mechanism involves the full length of the transmission lines connecting the substations of the RTS-96 system. E3 modeling is further explained in Section 4.2 and readers with interest in EMP E3 effects are pointed to [21].

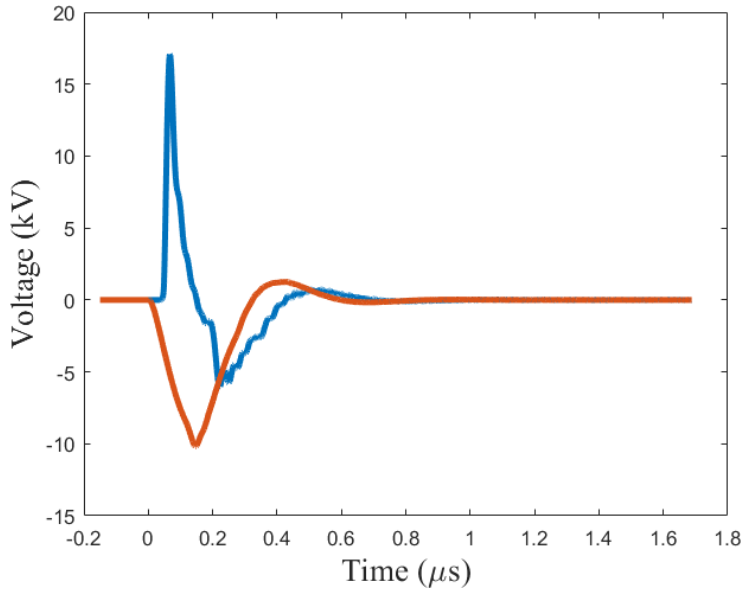

Figure 2-2. Two simulation examples of the E1 EMP induced voltage seen by a relay in an IEEE test system.

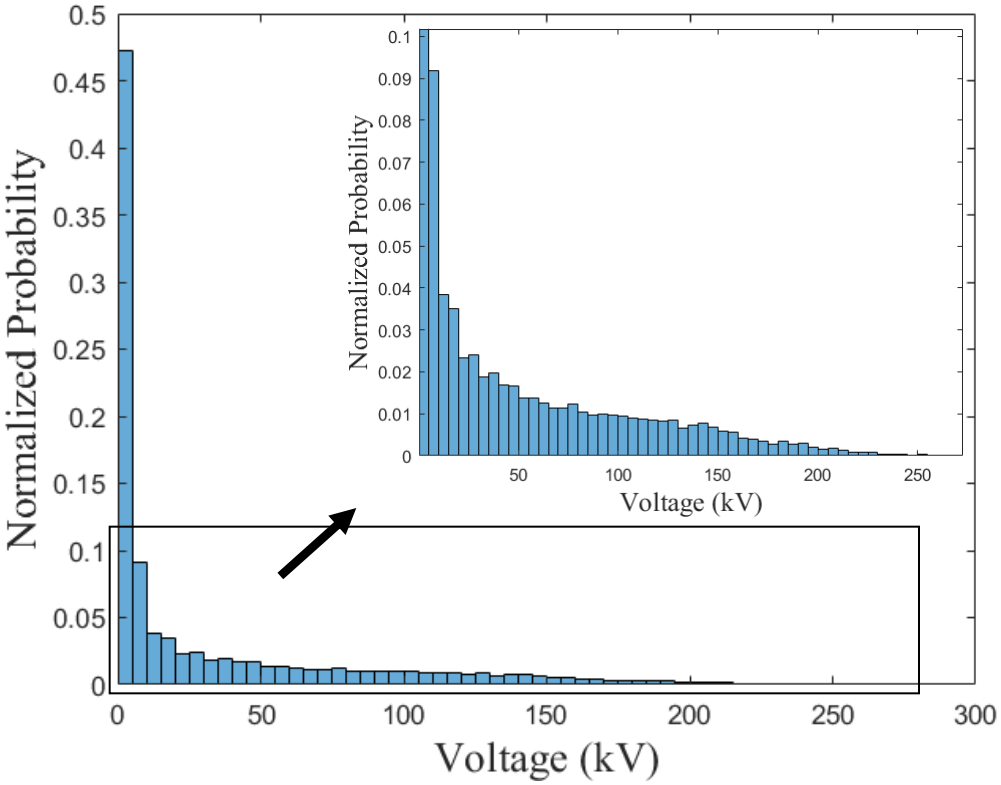

Figure 2-3. Histogram of E1 EMP induced max voltage levels at all the relays in an IEEE test system for 1000 synthetic HEMP scenarios.

3. COMPONENT TESTING AND FAILURE MODES

Sandia EMP testing and modeling is focusing on developing failure models for protective relays, current transformers, potential transformers, breaker trip and close coils, control circuit contactors, lightning arrestors, inverters, solar cells, dc-dc regulators, and power transformer insulation dielectric breakdown. Occasionally multiple components are connected in series to achieve one grid function, and if just one of those components in the series fails (the weakest link), that grid function will go offline. In other cases, grid components have redundancy, and a single failure may not cause a grid consequence. For these reasons, we must not only determine if a component fails, but how it fails, and what impact that failure will have on the grid.

The goal of the component testing is to create failure models that characterize the reaction of each component when insulted with an EMP. An example derived from initial relay testing in [22] is in Figure 3-1, where relays are subject to pulse injection tests with voltages ranging from 0 – 180 kV. The relays were either: 1) unaffected, 2) failed to continue to operate, but only needed a power cycle to work again, or 3) failed altogether and would need to be replaced. Either reaction 2) or 3) would result in unprotected equipment, which could be a major problem, especially when a large number of high value components are left unprotected. In addition, there is a chance (although small) that a relay affected by the EMP may cause the component it is protecting (e.g. transformer, transmission line) to trip.

In order to demonstrate the HEMP grid modeling framework, relay failures are the only component failures considered. Therefore, the results are not indicative of the total impact of a HEMP event on the grid. Additional component models need to be incorporated to achieve a more accurate estimate of the impacts of a HEMP event on the grid.

For each HEMP scenario, every relay in the system sees a coupled EMP E1 voltage profile at its input terminal. Based on Figure 3-1, for each HEMP scenario, every relay in the system either is temporarily offline, fully damaged and in need of repair or replacement, or unaffected. If the relay is disabled, it is given a small probability that it will trip the component it is protecting (this probability is varied, and results are analyzed in Section **Error! Reference source not found.** and 5.3 for low p robability and Section 5.4 for high probability). Note that initial testing in [10] indicates a *very* low probability of when the relay fails – the component it is protecting trips offline. However, to exercise the cascading outage framework, a higher than expected probability of component tripping is used. This is further discussed in Section 5. Relays and components are removed from service in thousands of HEMP scenarios using synthetic data on the IEEE Reliability Test System from 1996 (RTS-96). The RTS-96 system and the modifications and protection elements are further discussed in Section 4.1. The components are removed in our dynamic cascading failure simulations, discussed in the next section.

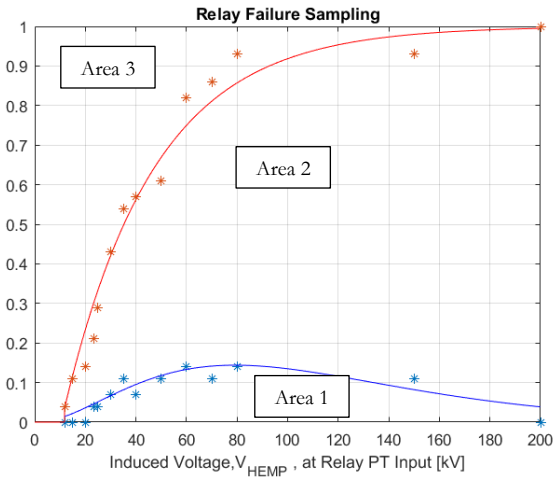

Figure 3-1. Relay failure sampling curve. Area 1 is the relay failed, but only needed a power cycle to continue to operate. Area 2 is the relay fully failed (permanently damaged). Area 3 is the relay operated normally. For Monte Carlo sampling, give a voltage level (e.g. 80 kV), a random number between 0 and 1 is selected (e.g. 0.5), and the relay reaction is dependent on where that point falls in the figure (e.g. 80,0.5 falls in Area 2, so the relay is permanently damaged). Derived from data in [22].

4. ELECTROMECHANICAL DYNAMIC TRANSIENT SIMULATIONS WHILE INCLUDING CASCADING FAILURES

The goal is to co-simulate power system dynamics during a HEMP event for both E1 effects and E3 effects. The methodology is summarized in Figure 4-1. Based on the HEMP event model discussed in Section 2, E1 caused components to be damaged or mis-operate, and therefore remove components from service in the electromechanical simulation. E3 simultaneously causes reactive power consumption at multiple buses due to transformer saturation throughout the system. The reactive power consumption causes low voltage problems at multiple buses. Combined, E1 and E3 can cause grid transients that may lead to large-scale problems or cascading failures.

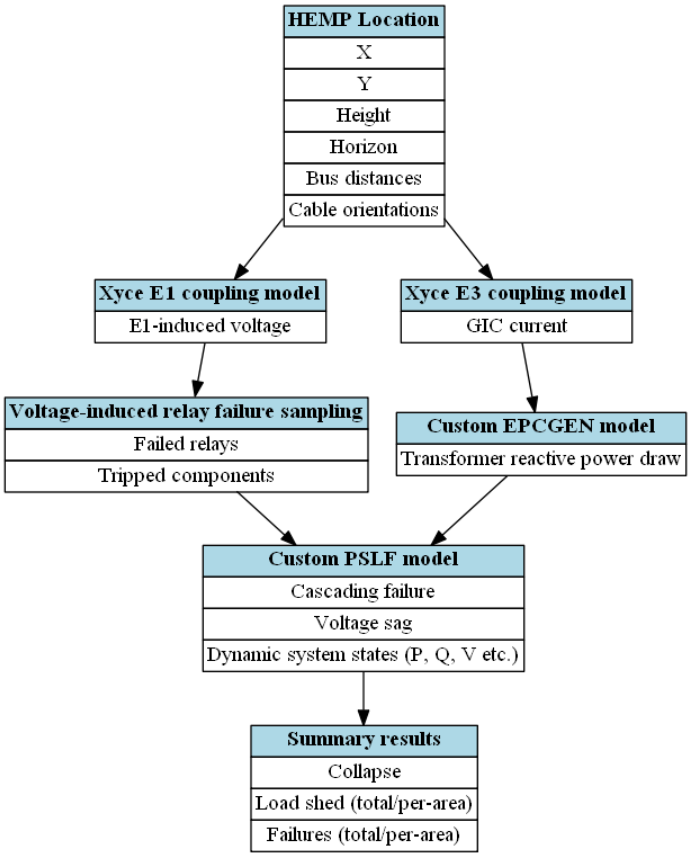

Figure 4-1. The power system co-simulation of EMP E1 and E3 methodology

4.1. The IEEE Reliability Test System (RTS-96) Modifications

The project team implemented the original RTS-96 system [23] in General Electric's PSLF platform and updated it to include grid dynamic models, which used data from the original RTS-96 publication [23], while including generator, governor, and exciter models with typical Western Electricity Coordinating Council (WECC) dynamic models and parameters. The RTS-96 is a three-area system, where all three areas are almost identical with a number of tie lines between the areas.

To create realism in the possibility and progression of cascading outages, protective relay models were added to the RTS-96 test system for the following areas: transmission line and transformer protection relays, under/over frequency and under/over voltage relays for all generators with tripping times set to WECC standards, and under frequency load shedding relays with settings set to WECC standards. All relays are assumed to have backup protection.

A. Generator Relays

Relays applied to generators included under and over frequency relays, and under and over voltage relays. Setpoints were selected based on [24] in Table 4-1 and
Table 4-2. Overcurrent and under excitation protection were not included in the simulation.

Table 4-1. Generator Under/Over Frequency Tripping

Frequency (Hz)	Tripping time (sec.)
61.7	Instantaneous
61.6	30
60.6	180
59.4 – 60.6	Continuous operation
59.4	180
58.4	30
57.8	7.5
57.3	0.75
57.0	Instantaneous

Table 4-2. Generator Under/Over Voltage Tripping

Voltage (pu)	Tripping time (sec.)
1.2	Instantaneous
1.175	0.2
1.15	0.5
1.1	1.0
0.9 – 1.1	Continuous operation
0.9	3.0
0.75	2.0
0.65	0.3
0.45	0.15

B. Under Frequency Load Shedding

Under-frequency load shedding relays were placed at all load buses. Since this model does not include subtransmission or distribution, it is reasonable to assume that under-frequency load shedding schemes would not trip the entire load offline, since such a load represents multiple substations, feeders, and loads. Values used to trip load offline were selected from WECC standard practices in [25] and are summarized in Table 4-3.

Table 4-3. Under Frequency Load Shedding Schedule

Frequency (Hz)	Percent of Load shed in the area	Tripping time (sec.)
59.1	5.3%	0.233 (14 cycles)
58.9	5.9%	0.233
58.7	6.5%	0.233
58.5	6.7%	0.233
58.3	6.7%	0.233
Additional load shedding to correct under-frequency stalling		
59.3	2.3%	15
59.5	1.7%	30
59.5	2.0%	60

C. Transmission Lines

Zone 3 impedance protection industry practice is to establish its impedance trip setpoint to correlate with 1.5 pu current and voltage at .85∠-30 degrees on its transmission line. This effectively implements Zone 3 as an overcurrent relay. For this reason, overcurrent relays are added at both ends of every transmission line and the overcurrent settings were based off the existing RTS-96 line ratings included in [23]. Due to the delay associated with Zone 3 backup, the overcurrent was required to be sustained for ≥ 2.5 seconds before a trip would occur. The clock associated with this delay reset every time the line current dropped below this rating, as is done in industry practice.

D. Transformers

Transformers are a critical and expensive grid component with long lead times for repair or replacement. For this reason, industry practice includes a comprehensive protection scheme for transformers. The only protection considered in this project is overload protection with backup protection. Overcurrent protective relays were added to the dynamic simulation. Ratings for the transformers are also included in [23], and relays are set to trip these transformers if the overcurrent persists for ≥ 2.5 seconds.

4.2. Modeling HEMP E3

The power system impacts of the late time component (Magnetohydrodynamic Electromagnetic Pulse or E3) of an EMP pulse were incorporated into the dynamic simulation. The E3 component can cause low-frequency, geomagnetically-induced currents (GIC) in lines and transformers. These GIC currents, as has been well documented regarding geomagnetic disturbances, can result in part-cycle saturation of transformers which can cause a variety of negative impacts. Note that a HEMP event can maximize E1 *or* E3, and often the part of the grid affected by E1 and the part affected by E3 are in different locations (that is, E1 and E3 might not overlap).

The focal point of the E3 simulations were to analyze voltage collapse due to increased reactive power losses within bulk power transformers subject to GIC. This did not include any thermal (hotspot) or harmonic impacts resulting from magnetic saturation of the transformer cores. The reactive power impacts were co-simulated with the E1 impacts as explained in Section 4.3.

4.2.1. RTS-96 E3 Impact Locations

The IEEE Three Area RTS-96 reliability test system [23] model was evaluated for candidate transformers potentially subject to GIC. Identifying potential paths for GIC in the model depended on transformer types and grounding. Wherever a complete grounded path between two transformers was assumed, GIC were assumed to be possible.

All transformers in the model were assumed to be either generator step-up (GSU) or Autotransformers. GSUs, as the name indicates, were assumed anywhere a transformer connected to generation asset(s) was used to connect to the higher transmission voltage, a total of 39. Autotransformers were assumed for all transformers connected between 230 kV and 138 kV, a total of 15.

The high side of all GSU transformers were assumed to be the grounded-wye side of the delta-wye grounded type assumed for all. The autotransformers were also assumed to be grounded, resulting in both the series and common windings of the autotransformers being considered conducive to GIC. Due to pairs of GSUs and autotransformers sharing common buses, it was possible to aggregate GIC

from two transformers into one representative sum on several buses in the model. A total of 51 buses were identified as locations to simulate reactive power loads, as shown in yellow in Figure 4-2.

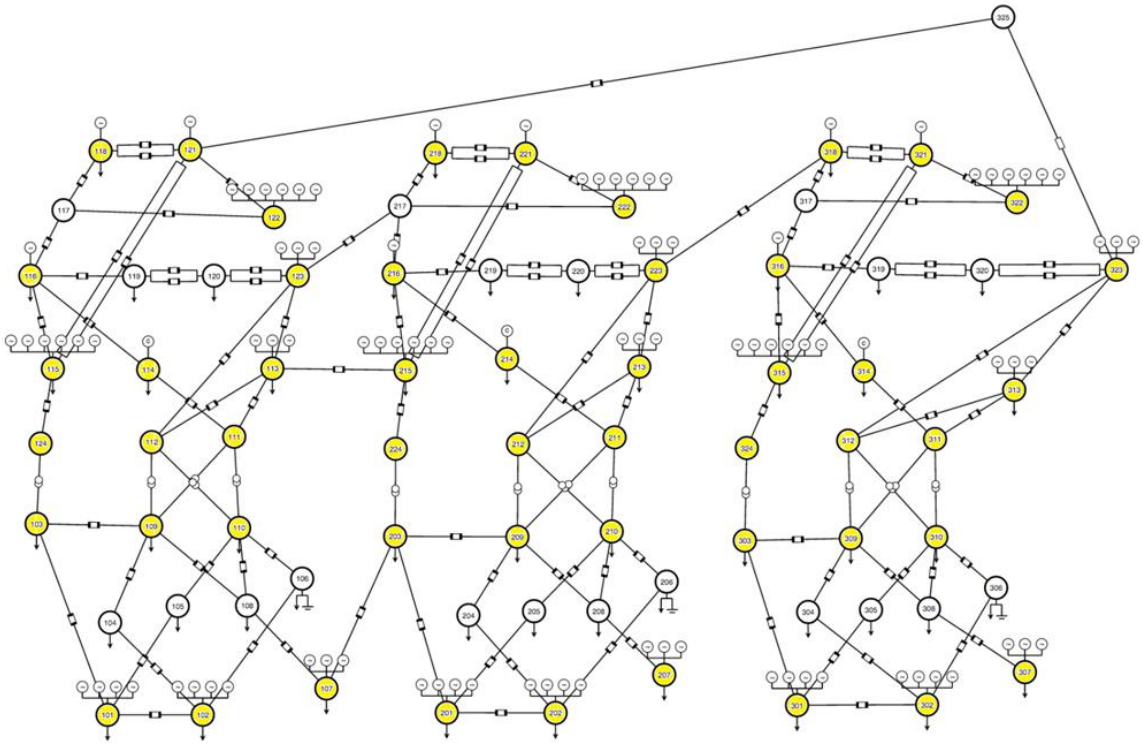

Figure 4-2. The RTS-96 Three Area system diagram [23] with reactive power burden locations highlighted in yellow.

4.2.2. E3 GIC Calculations

Using the line voltage coupling results in Section 2, GICs can be calculated using DC representations of the system [26]. DC resistances for the transformers were derived using the transformer equivalent circuit guidance in [27] and the parameters defined in the RTS-96 power flow model. As described in [27], a conservative (higher GICs) substation resistance of 0.1 ohms was assumed throughout the model. Xyce was then used to calculate the GICs, which were then collected at all elements necessary to properly represent the reactive power losses of all transformers of interest.

The GICs were saved to an external data file for each scenario to be used in the dynamic simulation. Each data file contained ~60 seconds worth of data for each of the 51 buses where reactive power losses were simulated. The GICs were calculated and recorded at 100 ms time steps. Net GIC values were calculated for buses with multiple transformers connected to them. The external data files were referenced from the dynamic simulation to ultimately calculated and implement the reactive power losses. The GIC current values at all 51 buses in the RTS-96 system for one exemplary synthetic HEMP scenario is in Figure 4-3.

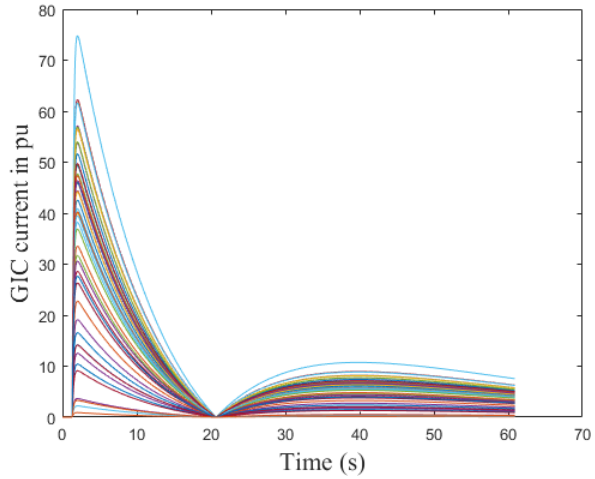

Figure 4-3. EMP E3 GIC current values at all 51 buses in the RTS-96 system for one synthetic HEMP scenario.

4.2.3. Reactive Power Loss Simulation

The ultimate parameter needed to simulate the E3 impacts of interest is the reactive power loss at each eligible location. Once the GIC are calculated, the reactive power losses can be calculated as in [28],

$$Q_{\text{loss,pu}} = V_{\text{pu}} K I_{\text{GIC,pu}} \tag{1}$$

where V_{pu} is the AC bus voltage in per unit, K is a dimensionless scalar dependent on transformer type, and $I_{\text{GIC,pu}}$ is the GIC through the transformer in per unit (three-phase equivalent). Figure 4-4 illustrates the E3 incorporation method at a high level.

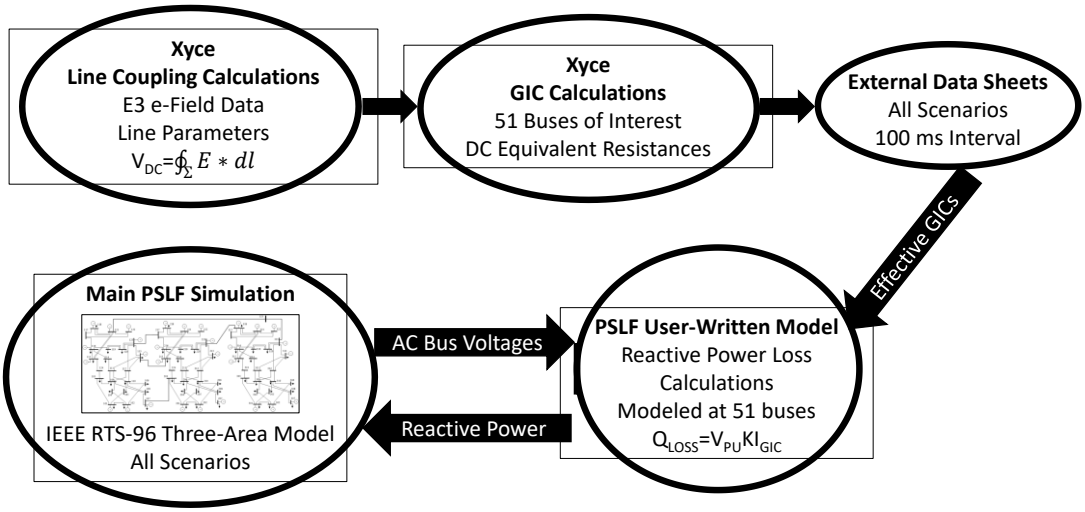

Figure 4-4. E3 impact incorporation overview.

The AC bus voltages are extracted from each of the 51 buses in the PSLF dynamic simulation at every time step, set at 100 ms, then the calculated reactive power load is returned. The PSLF "EPCMOD" and "EPCGEN" user-written models were used to manage external file importing and

reactive power loading in the simulation. Transformer details necessary to calculate more appropriate K factors for each unit were not available, therefore a conservative value of 1.5 was assumed, per [29]. The 51 buses in the RTS-96 system consume reactive power due to the EMP E3 event; this leads to voltage collapse issues throughout the RTS-96 system. Simulations are completed while considering only E3 impacts of the HEMP scenarios. As expected, many of the scenarios caused voltage degradation throughout the system, as seen in an example scenario in Figure 4-5, which confirm findings in [21]. Note, findings in [21] indicate worse voltage issues on the real systems compared to this test system. Many things may contribute to this difference, the EMP model, vastly different systems, line lengths, transformer resistance assumptions, ground conductivity assumptions, modeling of distribution GICs, different dynamic generator/exciter/governor models and parameters, and many other assumptions. A more comprehensive analysis may show much worse voltage suppression.

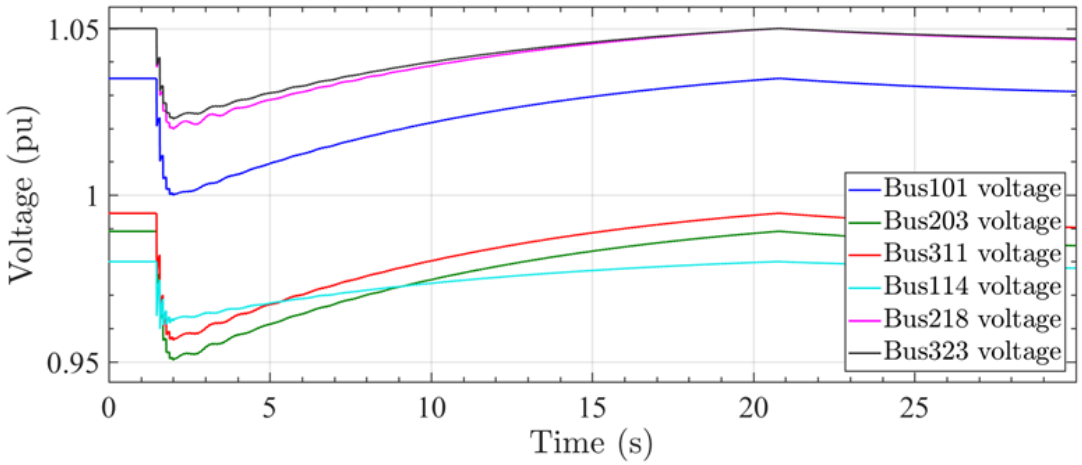

Figure 4-5. The voltage degradation due to EMP E3 transformer saturation at a set of buses in the RTS-96 system, for an exemplary HEMP scenario. Note, this is a result while considering E3 only impacts, and has many other assumptions built in.

4.3. Modeling HEMP E1 with E3

Once testing is finished and failure models are created for all the components, a Monte Carlo approach is used to determine the failed components during a HEMP scenario, and the failure mode. A dynamic power system modeling framework has been developed to determine the immediate grid consequences during a HEMP scenario. The dynamic power system model is meant to handle dynamics where a large number of components are removed from service, also known as N – k events (where N is the number of transmission level components in the system and k components are removed from service where $k > 2$).

After the failure model sampling process selects which components fail, the delay between the HEMP event and the grid reaction is selected with another Monte Carlo sampling. Although the E1 wave will have dissipated within microseconds, it may take some time for a damaged component to be realized on the grid due to communication delays, control delays, and time required for the failures to manifest. Further testing is needed to accurately identify this delay distribution for different failures. For initial testing a delay distribution is based on typical breaker operation times.

Once the sampling process is over, each HEMP scenario includes a list of components that trip offline due to E1 and a time at which they trip offline ($t_{trip} = t_{HEMP} + t_{delay}$). A power systems dynamic simulation is run for each HEMP scenario tripping components offline. In the dynamic power systems

model, a custom user defined model attempts to capture the effects of E3 over the course of the 45 second simulation. As components are tripping offline due to E1, reactive power consumption at transformers affected by E3 is causing voltage collapse in the system. Protection devices are included in the dynamic power systems model, this allows for cascading transients, and cascading outages to occur from the E1 and E3 affects.

This is a co-simulation of E1 and E3 to determine the consequences to the grid. Note there can be scenarios where the E1 and E3 components of the HEMP event do not overlap geographically; in these cases, single E1 or E3 component analysis will suffice. The system-wide results are analyzed with the primary goal of finding the most vulnerable points in the grid to HEMP events and determining the optimal investment locations to harden these vulnerabilities. Note that significant time domain data is saved for every HEMP E1-E3 scenario simulation, and data analytics is used to determine quantitative actionable results as discuss in Section 5. Multiple sets of 1000 HEMP scenarios are simulated and analyzed to gather trends, critical node information, and expected impact information. Section 5 describes the analysis framework to evaluate the results using advanced data analytics.

Following the dynamic simulation, the grid may not be at a stable point. For example, transmission lines may still be overloaded. For this reason, a security constrained ACOPF (or DCOPF) is run, with the objective to minimize weighted load shed and determine the longer-term outages from the HEMP event. The ACOPF will: 1) bring back components that tripped due to transients but not due to damage, 2) prioritize the restoration of critical loads, 3) ensure system voltages, line currents, and generation limits are within specification.

5. ANALYSIS FRAMEWORK – CRITICAL NODES, STATES, AND TRANSITIONS

We developed an analysis framework to discover patterns and mechanisms of cascading failure from stochastic simulation replicates. In our analysis framework, we viewed the entire set of available data for a simulation scenario – including initiating event (e.g., HEMP) characteristics, immediate topology and component impacts, cascading protection, and steady-state load shed – from a systems perspective. Various spatial and temporal combinations of failures can result in different degrees of disruption of the system, as measured by the total weighted load shed. The analysis framework can describe system level patterns and dynamics that tend to result in catastrophic failure, as well as identify critical nodes and states that are associated with significant grid disruption. In recognition of the fact that the dynamics of grid disruption of even small systems with few perturbations can result in complex and chaotic behaviors, we made use of the entire corpus of replicate simulations in an effort to find similarities between replicates that showed similar trajectories through time, and similar final states following disruption. In this way we hoped to characterize consequential components, critical states, and transitions using combinations of ordination, clustering flow analysis, and network theoretic approaches.

A key consideration in developing this framework was the expectation that low-probability, high-impact scenarios would be of special interest from an analysis perspective. That is, scenarios that demonstrate little or no impact to the grid do not warrant significant further analysis, whereas a set of stochastic scenarios with significant impacts may encode rich information about cascading failures, geographical distribution of impacts, unusual system operating modes, and key components that are more critical to system operation.

To develop and exercise a framework capable of analyzing systemic impacts, it was necessary to have a set of simulation results that exhibited such impacts. In the current incarnation of the simulation framework, component tripping due to E1 relay failure is a primary mechanism for causing disruptions. This is not to say relays are the main problem that may occur with EMP events, this was just the mechanism used to cause large-scale grid disruption scenarios to exemplify our analysis framework. To provide high-impact cases for analysis, we used notional data generated by greatly exaggerating the likelihood of relay failure causing a component trip. Whereas testing indicates that this phenomenon is possible but quite rare, the notional data analyzed within this section result from assuming a high (10%) or extremely high (100%) likelihood of component tripping upon relay failure.

Accordingly, while the results in this section demonstrate capabilities of the analysis framework, they are not representative of expected EMP impacts. However, both the simulation and analysis frameworks could be used to understand likely EMP effects if a more complete set of EMP-induced failure mechanisms and better information about device prevalence and trip probabilities is used. It is likely that with different system or HEMP characteristics, simulation scenarios resulting in significant systemic effects would be present in the results set. The notional results here demonstrate the types of analysis that are possible with sufficient samples of such high-consequence scenarios.

5.1. Data Processing and Preparation

We produced a data processing ETL (extract, transform, load) workflow to ingest and produce derivative metrics from large bodies of replicate PSLF simulations, preserving the HEMP data and simulation component status for all failures. In the summary files produced from this workflow, component failures due to E1 relay coupling as well as those due to subsequent cascading failure are produced for a user defined set of simulation times. The resulting capability allows the discrete

temporal analysis of an arbitrary number of temporal samples of the simulation output. The resulting ETL workflow is primarily the conversion of the simulation results, consisting of a series of proprietary MATLAB files and ancillary text files, which in aggregate constitute the HEMP location and characteristics, E1/E3-caused failures, and PSLF results, into a single comma delimited file.

We conducted all model parameterization and output analyses, as well as figure generation using Python (Python Language, version 3.7).

5.2. Synoptic Load Shed and Scenario Failure Distributions

In this section, notional results are presented that use the high (10%) probability of relay-caused tripping. With the E3 assumptions discussed above, E3 caused voltage suppression on the RTS-96 system (as seen in Figure 4-5). Accordingly, most disruptions in our synthetic scenarios are caused by the (exaggerated) phenomenon of E1 relay-induced tripping

Even at the high 10% assumption, load shed impacts were generally small. These impacts can mostly be attributed directly to relay-caused tripping. Of all failed lines and generators, few failed as a result of *cascading* dynamics following the EMP. However, for the small fraction of replicates that experienced cascading component failure and ultimately collapse, we detected some faint signals reflecting the underlying symmetry of the fictitious RTS-96 system. Figure 5-1 and 5-2 show a heatmap of generator and line failures through time. The symmetry present in generators at buses in this model system highlights the potential for functional equivalence in highly symmetric systems and merits more investigation.

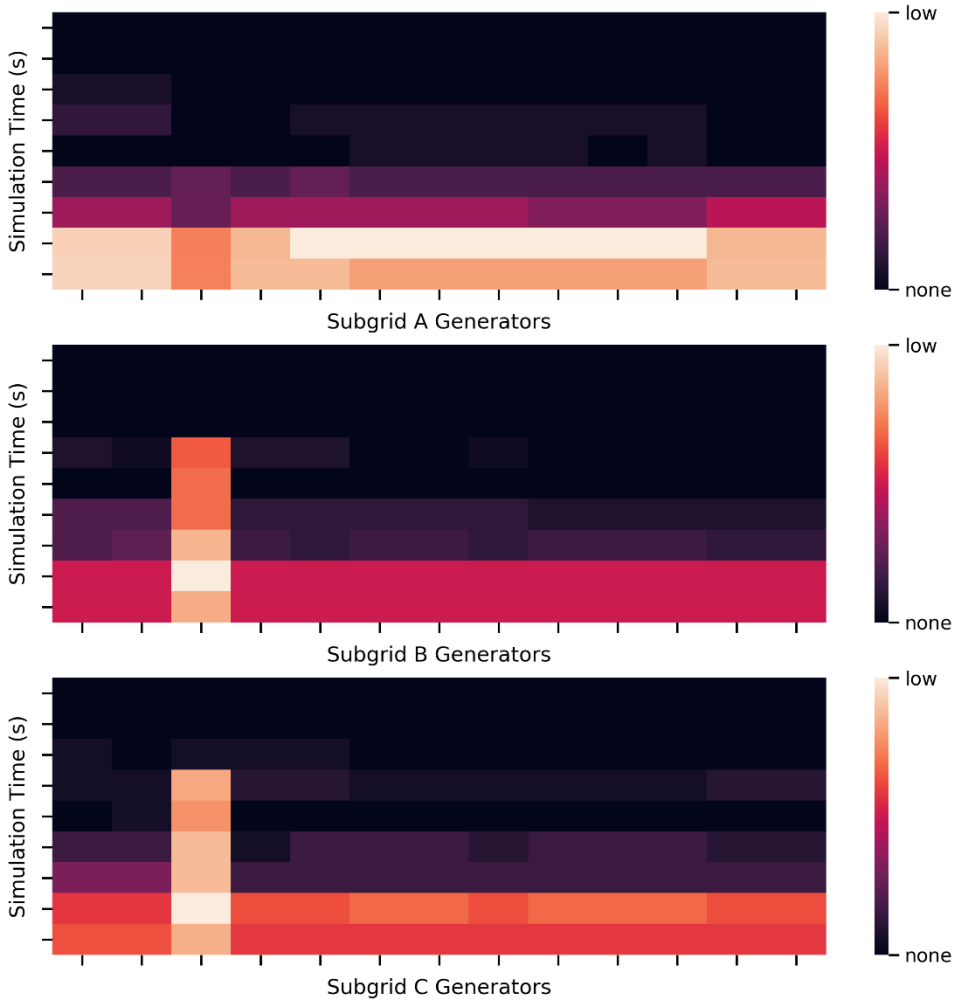

Figure 5-1. Number of failures for generators in the RTS-96 system through time, for the 1000 E1 + E3 scenarios sampled. Lighter colors indicate more component failures. Each plot describes the likelihood of failure of generators for each subgrid A, B, and C. Note the Y-axis is non-linear, ranging from PSLF simulation start (top) to finish (bottom).

We then calculated the odds ratio for generator and line failures and system collapse across a series of temporal slices from 0-30 seconds (Figure 5-3). Warmer colors indicate a higher likelihood that failure of the component would result in total system collapse. It should be noted that the signal-to-noise ratio of this effort is markedly small given the small number of component failures, and even smaller fraction of replicate simulations that resulted in system collapse. Much like the results from the failure probability analysis, the odds ratio results were suggestive that certain components were more participative in system collapse, with the same general patterns present in the individual component failure probability results shown in Figures 5-1 and 5-2, further strengthening the notion of symmetry or functional equivalence across the 3 areas of the system.

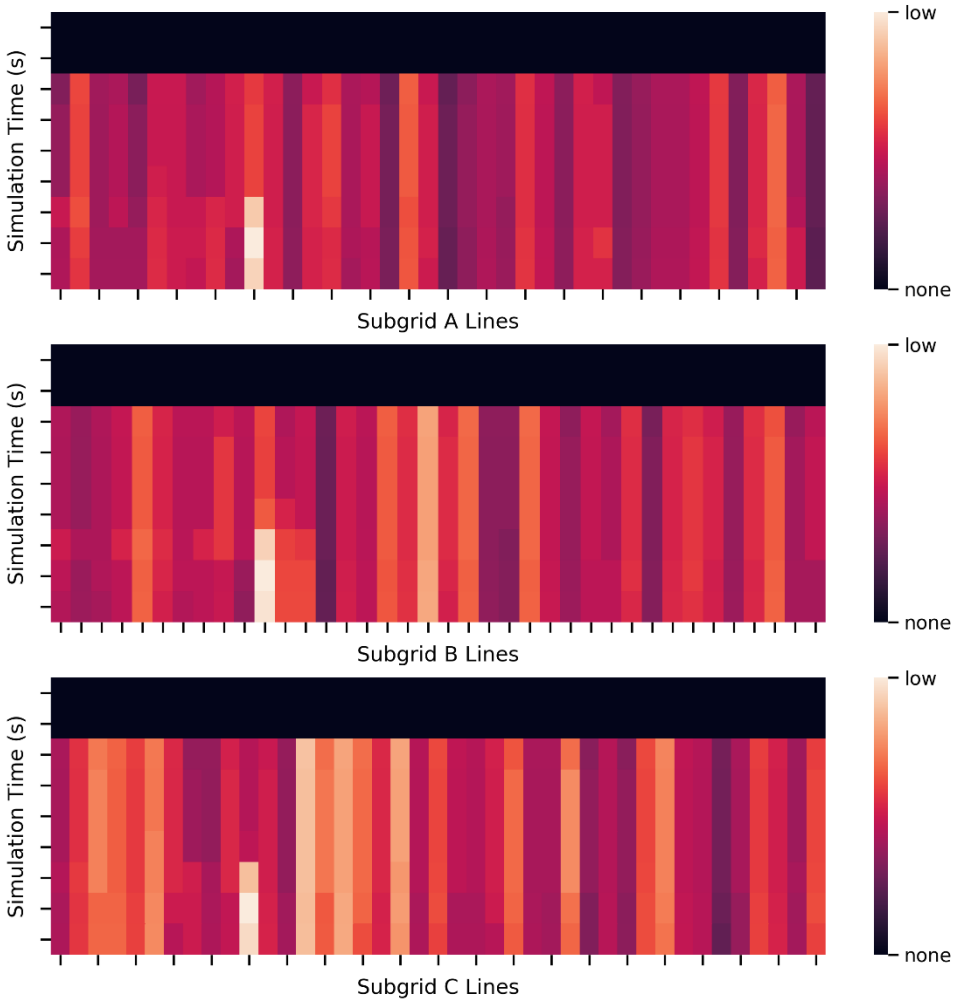

Figure 5-2. Number of failures for lines in the RTS-96 system through time, for the 1000 E1 + E3 scenarios. Lighter colors indicate more component failures. Each plot describes the likelihood of failure of lines for each subgrid A, B, and C. Note the Y-axis is non-linear, ranging from PSLF simulation start (top) to finish (bottom).

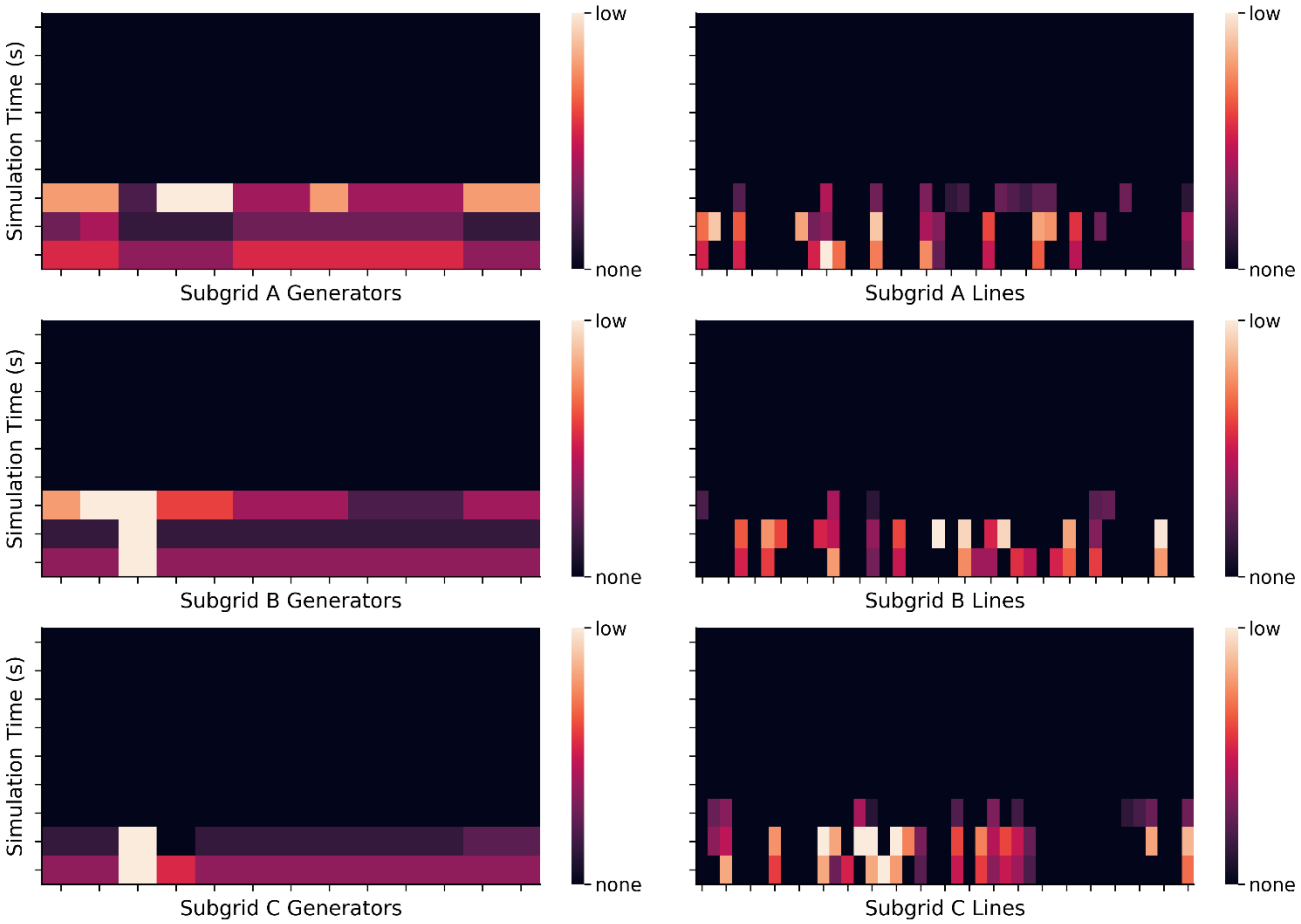

Figure 5-3. Odds ratio calculation for generators (left) and lines (right) in the RTS-96 system through time, for the 1000 E1 + E3 scenarios. Lighter colors indicate a higher likelihood that component failure will result in a system collapse.

Beyond the observation that specific components with similar topology across the three subgrids both fail more frequently and are more often involved in cases of system collapse, there were also broad patterns of regional activity and inactivity. Figure 5-3 highlights these findings, where for instance the nature of line failures involved system collapse in subgrid C appears more clumped than those in subgrids A or B. The presence of these trends, albeit with incredibly low signal, suggests that further research seeking to understand how topology affects component failures, and the level of involvement of those failures in system collapse is needed.

5.3. Critical System States and Transitions

We sought to characterize the disruption of the network in terms of its topological state and state transitions through time. We conducted a temporal clustering analysis of the 1000 replicate simulations for each scenario using hierarchical aggregated clustering of the line and generator status (online or failed) for the entire corpus of simulation results. In an effort to discretize the topological states temporally, we assigned the cluster membership to each replicate simulation across a series of temporal slices. In this way, we can make the claim that a simulation that saw no topological perturbation would

retain the same cluster identity across the temporal slices. However, simulations that saw disruption due to the EMP coupling or subsequent cascading simulation failure would be assigned to a different cluster across the temporal gradient. Further, our initial clustering using the entire replicate and temporal space helped preserve the notion of similarity between cluster attributes across the temporal gradient (i.e., cluster 4 at time 5 and cluster 5 at time 20 are likely to have related topological traits).

While the clustering effort categorized similar system states (topology, generator status, and load status), we acknowledged that the consequence of state membership in a cluster at different points in time could be predictive of end-of-simulation status of the system. Consequently, we conducted a clustering analysis across 9 temporal slices (0, 1, 2, 3, 4, 5, 10, 15, and 20 seconds), where at each slice we clustered the replicates based on their line topology and generator status. We then organized the clusters as a Sankey diagram (Figure 5-4), where nodes corresponding to cluster assignments, and edges corresponding to the number of replicate simulation transitions between states.

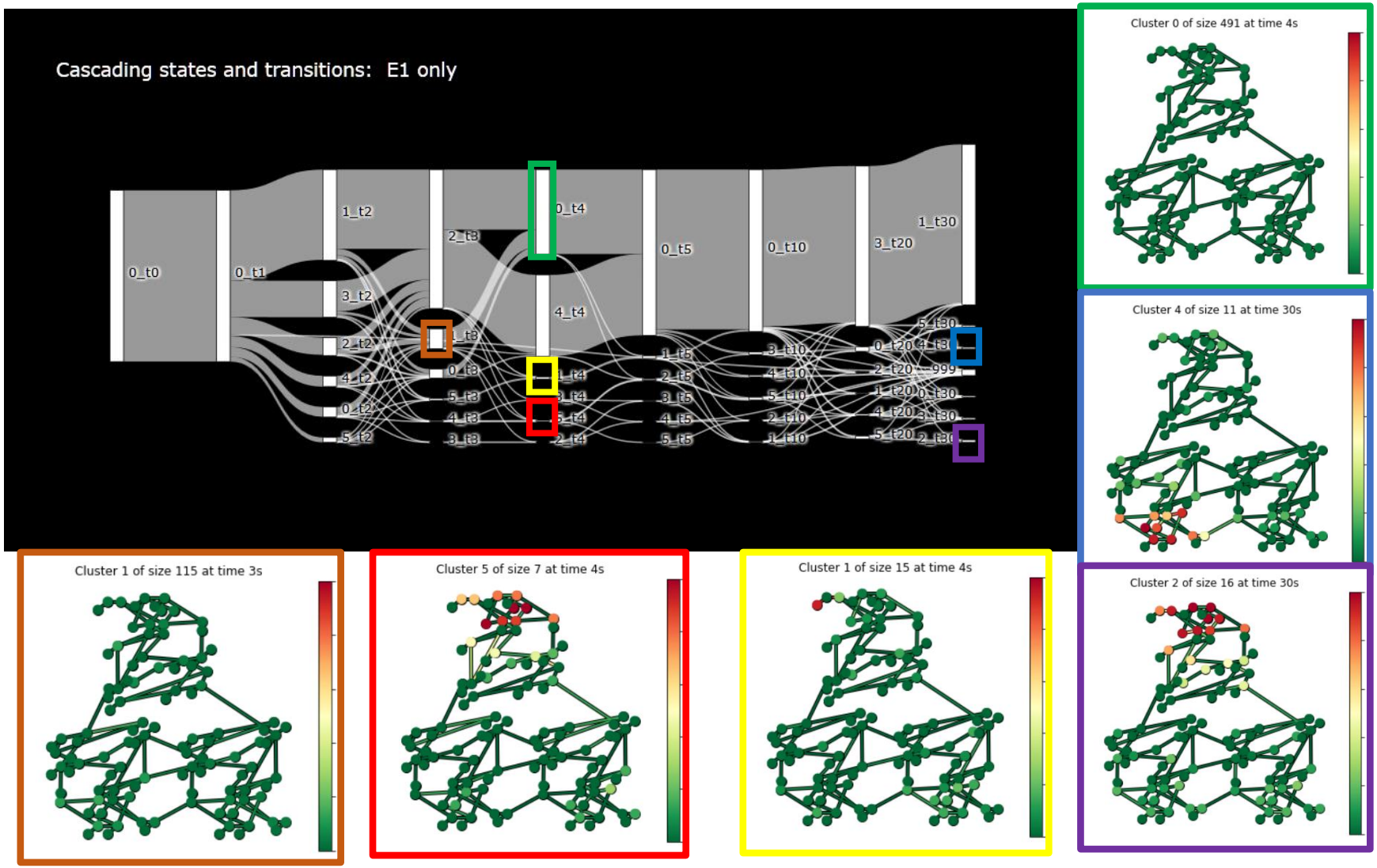

Figure 5-4. Temporal clustering analysis of the scenario replicates, with state transition flow width proportional to the number of replicates whose cluster assignment changed accordingly. Example cluster characteristics (load shed, line failure probabilities) are highlighted in the margin, with color coded extents matching the box labels on the Sankey diagram.

Here the flows are computed as the number of replicates in cluster A at time T that transition to cluster Y at time T+1. The total number of replicates are preserved through this process. Additionally, we create a terminal node for collapsed simulations, where any simulation that had collapsed between time T and time T+1 is added to the flow to the collapse cluster.

In our simulations, failures caused directly by the EMP take place between 1 and 2 seconds after the simulation starts, accounting for the high degree of activity in state transition during the early time periods. Included in the figure margins are representative outage maps for the scenarios that make up the color-coded clusters. Of particular interest is the high degree of regional failure in the corresponding clusters. Further, it should be noted that no information about load shed was used to drive the clustering results. The patterns in apparent load lost at each node in the network were emergent properties of the system state disruption of the network, specifically in terms of topology and generator status.

5.4. Implications for High Component Failure Scenarios

The patterns and trends in load shed and component failures we characterized above were characterized broadly by a relatively small amount of depreciation following the EMP coupling with the grid, despite the heavily exaggerated 10% probability of tripping upon relay failure. This challenging signal to noise environment made identifying specific critical grid elements (e.g., nodes, edges) with statistically meaningful thresholds a difficult task. However, we conducted some exploratory experimentation with a small subset of simulations with more pessimistic relay failure assumptions, and subsequently a significantly greater number of component failures and collapsed scenarios. The consequence of these increased acuity scenarios was a higher signal to noise analysis environment, enabling the stronger description of critical states and components in the simulations. Thus, while the results are not representative of realistic EMP impacts, they demonstrate capabilities for analyzing a body of stochastic simulation results that includes multiple high-impact scenarios.

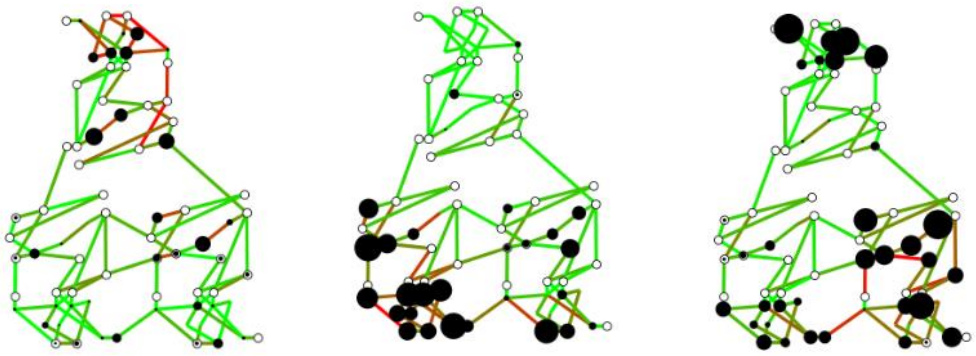

Figure 5-5. Cluster analysis of load shed (node size) and line failure probability (edge color) as an illustration of the end of simulation system states in the high failure probability experiments.

Figure 5- illustrates three of the regionally focused clusters we identified at the end of the simulation, with line failure probabilities characterized by line color, and bus load shed characterized by node size. A summary graph of the load shed by cluster (Figure 5-) highlights the distribution in load lost at the system level (orange dots) with those lost in the three symmetric sub networks, for 10

clusters (3 of which are illustrated in Figure 5-) This load shed distribution by simulation cluster shows us how the functional consequences of component failure in regionally discrete areas of the grid fall out on the distribution of replicate simulations.

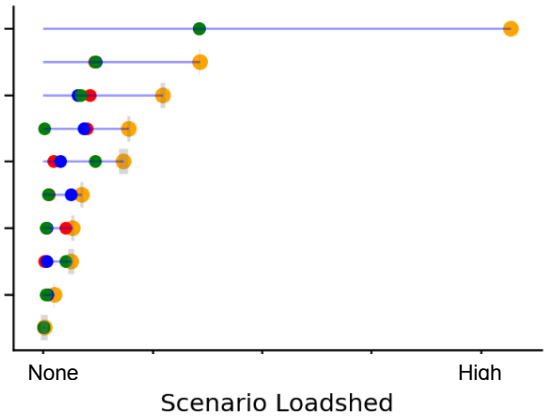

Figure 5-6. Load shed by RTS-96 sub-network, for 10 distinct clusters of simulation. Orange dot is the load shed total across all subgrids. Red, blue, and green dots are load shed in each subgrid (area).

When we performed an ordination on line and generator status using t-SNE, the distinct groups that manifest from this compression of dimensionality become apparent (Figure 5-), and further suggests that distinct trajectory "modes" exist, and some seem to have much stronger association with collapse or significant load shed than others.

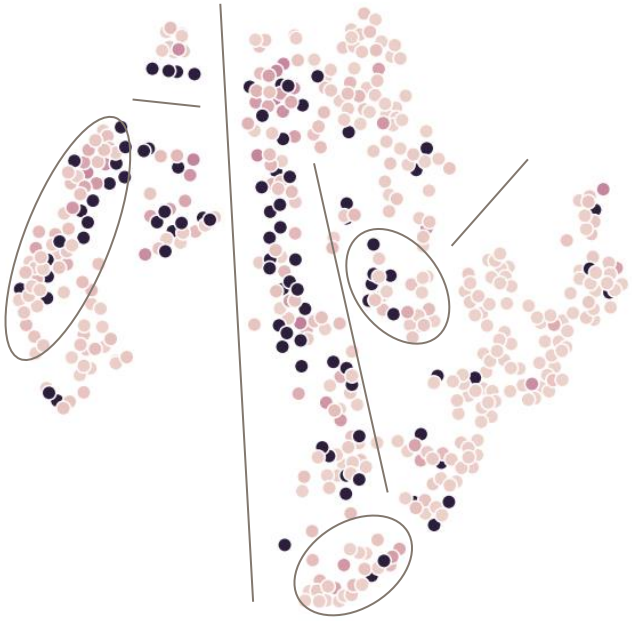

Figure 5-7. DEF - t-SNE ordination of the high failure rate experiments. Each dot represents a synthetic scenario. The x and y dimensions were defined by all line and generator states at the end of the simulation. Point color ranges from no load loss (pink) to total loss of load (black). Lines to visually accentuate group separation.

We pursued this notion that distinct failure modes exist, and are associated with varying degrees of load shed and collapse likelihood by conducting separate k-means clustering across all the high failure probability replicates on the X, Y, and Z coordinates of the EMP detonation, the line and generator failures, and on load shed. Consequently, for each of those three clustering criteria, we assigned each replicate simulation to one of ten k-means determined groups. We were interested in understanding if group membership in, for instance, a specific EMP location cluster was indicative of either how many components tripped, or how much load shed the system experienced.

In the Sankey diagram in Figure 5-, we show that particular system modes are associated with each other, indicating that causal inference may be further possible given the correct ordination and clustering axes. Future work will include analyzing the strength of association between these clusters via calculation of the odds ratio of simulation replicate assignment to any pair of clusters (e.g., EMP cluster 0 and the minimal load shed cluster). Earlier regression analysis showed that load shed cluster can be predicted with a fair degree of accuracy based solely on EMP location and component trip cluster assignment, lending credence to the hypothesis that there is some predictable causality between (at least some) EMP location modes, component trip modes, and final load shed pattern. Furthermore, distinct failure and system behavior characteristics of each cluster may be discoverable through statistical tests.

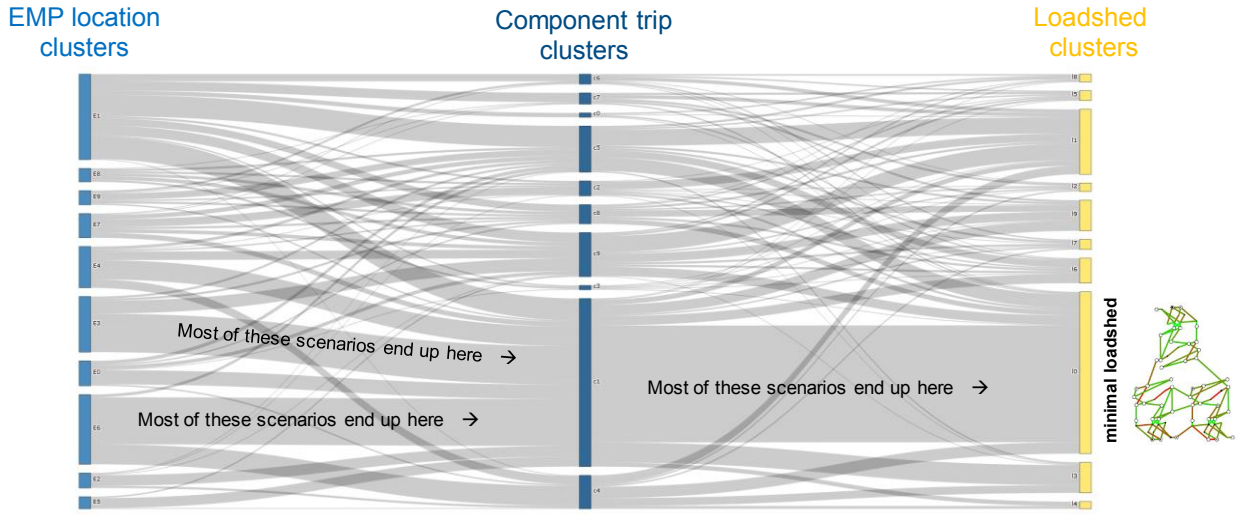

Figure 5-8. Sankey diagram relating the k-means governed group membership of EMP location, component failures, and system load shed. Each column breaks 500 synthetic severe replicates into ten group labels.

We were able to identify some synoptic patterns in the data which were not initially evident in the lower failure rate experimentation described above. While intuitive, we identified that the coupled voltage, and the likelihood of component failure, at electrically adjacent buses was correlated. Further, we determined that buses in areas A and B are coupled strongly internally *and* to each other, whereas area C is strongly coupled mostly internally. Load shed at some buses were strongly correlated with the load shed in the area they occupy; this finding was driven primarily by collapse – either the bus and the area survive, or the bus and area fail. Further investigation here may be valuable to understand why some buses appear to be robust to load shed, up to the point of area-wide collapse.

Given the greater likelihood of component failures in this experiment, we were able to speak to the causal inference capability of knowing the state of the system, in terms of the system topology and generator status. We determined that the number of relay-caused trips in the system had strong

association with whether or not the system shed substantial load, but this is likely very dependent on the grid under test and would be interesting to study further from a hazard-agnostic *n-k* survivability perspective.

Further, some high-level topology insights became evident. We found strong associations between certain load shed patterns and the number of transmission lines failed in certain areas. Specific transmission lines emerged as having greater importance; for example, failure of each of the lines between grid areas greatly increased the likelihood of substantial load shed. While largely intuitive, these results indicate that electrical connection-centric investigations may yield further constructive insights capable of generalizing to more complex and low failure likelihood systems. We further found evidence that some component failures are associated with serious systemic impacts (for example, failure of a specific transformer may be associated with a substantial increase in likelihood of system collapse), supporting the idea that critical components can be identified if sufficient samples are taken of moderate- to high-impact scenarios.

Ultimately, our high failure probability case study investigations still suffered from an inability to sufficiently sample across the massive sources of uncertainty. However, by artificially increasing the failure probability rate, we were able to essentially increase the signal to noise ratio of our experiment, by driving more components to failure and promoting greater system disruption. The inferences we drew from this subset of simulations are necessarily broad, yet we believe they demonstrate the capability to investigate the complex and chaotic system dynamics of cascading grid disruption in a reproducible manner. Future studies should focus on structuring the simulation characteristics such that the cascading sources of uncertainty resulting in the various conditional draws from distributions required to initialize the electromechanical dynamic simulations are well sampled, and result in sufficient signal to permit mechanistic, causal inference.

5.5. Sources of Cascading Uncertainty

This task was resourced to achieve the goals of creating a HEMP simulation and analysis framework. Deep, rigorous study of uncertainty propagation and quantification was beyond scope and is an intriguing area for further study and investment.

There are many sources of uncertainty in this problem. First are uncertainties about the system itself. The topology and operating/loading conditions of the system may matter considerably to HEMP survivability. For this study, the canonical RTS-96 configuration and power flow were assumed. Then, the geographical orientations (e.g. degrees from North) of sensor cables affects how the E1 signal couples into them. For a real system this information could be obtained (albeit at nontrivial effort/expense); for the RTS-96 system a notional random configuration was used.

The HEMP event itself and its effects on the system are a second source of considerable uncertainty. The HEMP location is uncertain and determines the bus distances and cable orientations (to the blast) used for the E1 and E3 coupling models. Then, for a given induced voltage level, a grid component has a certain probability of failure (an example seen in Figure 3-1), introducing component failure uncertainty. In addition, there is high uncertainty whether other grid components would go offline due to a HEMP. This introduces a considerable amount of uncertainty as to which components are tripped. Finally, the order and timing of component trips is determined via sampling from a beta distribution; while initial investigation indicates that trip order/timing has relatively minimal impact (over a one-second trip window), more thorough study would be appropriate. While other HEMP phenomena may introduce other uncertainties, they were not included in scope of the study due to lack of necessary information or deemed to have minimal effect or were otherwise.

Of these sources of uncertainty, perhaps the most problematic are those events which are binary, such as whether a relay failure causes a trip. These are problematic because they pose a combinatorics problem. For example, if x relays fail, each with probability y of tripping the circuit breaker, there are 2^x possible trip scenarios. Each of these scenarios has the potential for a fully unique outcome; even among n-k failure scenarios with the same k, outcomes may vary widely. For large x, unless y is very close to 0 or 1, any single sample will likely choose an n-k scenario that represents a vanishingly small portion of the overall probability space, and is likely not even representative of other n-k scenarios for the same k. This becomes particularly problematic in large systems, where estimation of anything beyond the mean impact requires an enormous number of samples.

The current stochastic simulation analysis work was limited by computational and time constraints on the number of stochastic simulations that could be run. Given appropriate inputs and assumptions, and a high number of samples, the framework presented would likely be sufficient to provide some insights regarding the diversity of possible EMP outcomes, a reasonable estimate of average load shed, and a rough characterization of system-wide load shed outcome distribution. However, the sample size needs to be greatly increased to deeply understand the plethora of system behavior modes or to develop the kinds of causal inferences that would be of interest for prioritizing system modifications or component hardening.

An obvious improvement would be to run significantly more samples using high performance computing resources. Even so, more rigorous deliberate study of the cascading certainties mentioned above, and their impacts on the results, is called for. This work should be guided by sensitivity analysis and make use of more sophisticated sampling methods where appropriate. One of the most significant challenges is in adequately representing the combinatorial space of possible component trip scenarios. One idea perhaps worth consideration is to perform stepwise adaptive simulation experiments, iteratively selecting the most impactful n-k events for consideration of n-$(k+1)$ events, to understand worst-case scenarios. This would provide (hazard-agnostic) insights into worst-case scenarios. This could perhaps be reconciled with realistic failure rates for the specific hazard (e.g., EMP) to provide upper-bound impact estimates, although the exact reconciliation mechanism is a matter for further study. Research into sophisticated surrogate modeling methods is of interest.

6. CONCLUSIONS

We have presented a framework for evaluating impacts of HEMP scenarios on a transmission-level power system. This report focused on the overall framework rather than specific results. This framework demonstrates the capability for modeling HEMP E1 and E3 effects. Specifically, E1-induced voltages (via coupling into sensor cables) are calculated and used to sample probabilistic component failures, while geomagnetically-induced current due to E3 causes a DC offset and reactive power draw at the transformers (and thus voltage suppression in the system). These effects are then simulated for thousands of HEMP scenarios on the IEEE RTS-96 synthetic dynamic electromechanical model with protective relays, allowing for cascading failure dynamics.

The results are analyzed with advanced analytics to help determine critical nodes and system behaviors. The analysis framework can describe system level patterns and dynamics that tend to result in catastrophic failure, as well as identify critical nodes and states that are associated with significant grid disruption. The specific results shown in this report are not indicative of actual HEMP impacts, rather the framework is presented while using synthetic data, on a synthetic grid, with assumptions to exercise the framework.

Adequate sampling over the many uncertainties involved is expected to result in a rich dataset of EMP characteristics, data on induced and cascading failures, and dynamic and final system state information. This data can be used to understand average behavior and characterize distribution of outcomes, e.g. system-wide load shed. Conceptually, this data can further be analyzed for key trends, behavior modes and critical components. A low incidence of HEMP scenarios with significant impact inhibited discovery of statistically significant causal/correlative effects in our base case. However, we were able to demonstrate promising methods for discovering key insights on an excursion with greatly increased failure rates. That is, it is easier to identify trends and critical nodes for higher impact scenarios.

Overall this framework shows promise in analyzing the grid impact from HEMP events and could be leveraged to analyze cascading events from other manmade or natural disaster high-impact scenarios. To accurately use this framework, the input data for all specific grid component failures from HEMP scenarios is needed; including if they fail, how they fail, at what time they fail, and the effect it will have on the bulk electric system model. Future research aims to significantly expand this framework.

REFERENCES

[1] C. Longmire, "On the Electromagnetic Pulse Produced by Nuclear Explosions," *IEEE Transactions on Antennas and Propagation,* vol. AP-26, no. 1, pp. 3-13, 1978.

[2] W. Radasky, "Introduction to the special issue on high-altitude electromagnetic pulse (HEMP)," *IEEE Transactions on Electromagnetic Compatibility*, vol. 55, no. 3, pp 410-411, 2013.

[3] R. Guttromson et al., "Electromagnetic Pulse – Resilient Electric Grid for National Security: Research Program Executive Summary," Sandia National Laboratories, SAND XXXX. 2020.

[4] T. Minteer, T. Mooney, S. Artz, D. E. Whitehead, "Understanding design, installation, and testing methods that promote substation IED resiliency for high-altitude electromagnetic pulse events," Proceedings 70th Annual Conference for Protective Relay Engineers (CPRE), 2017.

[5] Y. Zhou, Y. Xie," Comparison of analytical descriptions for early time high-altitude electromagnetic pulse waveform (E1)," Proceedings International Conference on Electromagnetics in Advanced Applications (ICEAA), 2016.

[6] "Electromagnetic compatibility (EMC) - Part 2: Environment - Section 9: Description of HEMP environment - Radiated disturbance," IEC 61000-2-9, 1996.

[7] R. Lee, K. Shetye, A. Birchfield, T. Overbye, "Using Detailed Ground Modeling to Evaluate Electric Grid Impacts of Late-Time High-Altitude Electromagnetic Pulses (E3 HEMP)," *IEEE Transactions on Power Systems,* vol. 34, no. 2, pp. 1549-1557, 2018.

[8] T. Hutchins, T. Overbye, "Power system dynamic performance during the late-time (E3) high-altitude electromagnetic pulse," Proceedings IEEE Power Systems Computation Conference (PSCC), 2016.

[9] D. Sanabria, "Early Time (E1) Electromagnetic Pulse Effects on Lightning Surge Arresters and Trip Coils," University of New Mexico, 2020.

[10] A. Baughman, et al., "HEMP Testing of Substation Yard Circuit Breaker Control and Protective Relay Circuits," Sandia National Laboratories, SAND2020-9872, 2020.

[11] T. Bowman, et al., "High Altitude Electromagnetic Pulse Testing of Photovoltaic Modules," Sandia National Laboratories, SAND2020-XXXX, 2020.

[12] A. Fierro, "Effects of EMP Testing on Residential DC/AC Microinverters," Sandia National Laboratories, SAND2020-9847, 2020.

[13] V. Greetsai, et. al., "Response of long lines to nuclear high-altitude electromagnetic pulse (HEMP)," *IEEE Transactions on Electromagnetic Compatibility*, vol. 40, no. 4, pp 348-354, 1998.

[14] United States of America Department of Defense Interface Standard, "High-Altitude Electromagnetic Pulse (HEMP) Protection for Ground-Based C4I Facilities Performing Critical, Time-Urgent Missions," MIL-STD-188-125-1, 1998.

[15] R. Araneo, S. Celozzi, "Direct time-domain analysis of transmission lines above a lossy ground," *IEE Proceedings Science, Measurement, and Technology*, vol. 148, no. 2, pp. 73-79, 2001.

[16] D. Higgins, T. Tumolillo, W. Radasky, K. Smith, J. Wondra, "Source Region EMP Coupling to Long Lines," *IEEE Transactions on Nuclear Science*, vol. NS-28, no. 6, 1981.

[17] IEC Technical Standard 1000-2-9, edition 1, 1996.

[18] Xyce, "Parallel electronic simulation," Sandia National Laboratories, available at: https://xyce.sandia.gov/.

[19] S. Campione, L. K. Warne, M. Halligan, O. Lavrova, L. San Martin, "Decay Length Estimation of Single-, Two-, and Three-Wire Systems Above Ground Under HEMP Excitation," *Progress in Electromagnetics Research B*, vol. 84, 23-42, 2019.

[20] R. L. Schiek, C. Lam, R. Beacham, G. Wright, I. Thruston, "EMP to Transmission Line Coupling and Lightning Surge Arrestor Energy Deposition," *JRERE,* vol. 38, no. 1, pp. 215-224, 2019.

[21] R. Horton, "Magnetohydrodynamic Electromagnetic Pulse Assessment of the Continental U.S. Electric Grid: Voltage Stability Analysis," Electric Power Research Institute Technical Report, 2017.

[22] "High-Altitude Electromagnetic Pulse and the Bulk Power System: Potential Impacts and Mitigation Strategies," Electric Power Research Institute Technical Report, 2019.

[23] C. Grigg *et al.*, "The IEEE Reliability Test System-1996. A report prepared by the Reliability Test System Task Force of the Application of Probability Methods Subcommittee," in *IEEE Transactions on Power Systems*, vol. 14, no. 3, pp. 1010-1020, Aug. 1999.

[24] N. A. E. R. Corporation, "Standard PRC-024-2 Generator Frequency and Voltage Protective Relay Settings," May 29, 2015.

[25] Western Electricity Coordinating Council Off-Nominal Frequency Load Shedding Plan, 2011.

[26] R. Horton, D. H. Boteler, "Calculation of GIC in Bulk Power Systems," 2013 Grid of the Future Symposium, Boston, 2013.

[27] R. Horton, "Magnetohydrodynamic Electromagnetic Pulse Assessment of the Continental U.S. Electric Grid – Geomagnetically Induced Current and Transformer Thermal Analysis." Electric Power Research Institute Technical Report, 2017.

[28] T. R. Hutchins, T. J. Overbye, "Power system dynamic performance during the late-time (E3) high-altitude electromagnetic pulse," IEEE Power Systems Computation Conference (PSCC), 2016.

[29] R. Horton, "Magnetohydrodynamic Electromagnetic Pulse Assessment of the Continental U.S. Electric Grid – Voltage Stability Analysis." Electric Power Research Institute, 2017.

[30] Y. Bai, H. Ding, S. Bian, T. Chen, Y. Sun, W. Wang, "SimGNN: A Neural Network Approach to Fast Graph Similarity Computation," Proceedings International Conference on Web Search and Data Mining (WSDM), 2019.

APPENDIX A – DEEP LEARNING FOR NETWORK TOPOLOGY SIMILARITY

The diverse set of grid component disruptions, while highly complex, may result in a small number of discrete critical failure modes. As described previously, the bulk of our effort to describe these failure modes focused on comparing network attributes at various simulation times for replicates with similar outcomes. So, the failure modes are expressible as simulation replicate clusters whose membership is determined via multivariate unsupervised temporal classification. As an exploratory effort, however, we sought to determine cluster membership of specific network topologies independent of the simulation consequences associated with network disruption. Consequently, we selected a graph similarity approach. This appendix attempts to employ SimGNN [30] graph edit distance (GED) to our grid topology data. However, it is shown that certain aspects of this algorithm do not translate well to our data set.

Graph similarity is a conventionally challenging, yet operationally valuable problem. Computation of most graph similarity metrics, like graph edit distance (GED) or maximum common subgraph (MCS), is NP-complete. Indeed, even the most current algorithms cannot, in reasonable time, compute the GED for pairs of graphs with more than 16 vertices (the RTS-96 network boasts 112 vertices, including generators). Speedier heuristics exist for approximating these similarity metrics, but they still suffer from unwieldly runtimes.

Deep learning approaches to this problem have been shown to circumvent some of the previously described problems by parallelizing computation to reduce runtime. Indeed, the runtime for deep learning networks trained to compute graph similarity metrics is less sensitive to increase vertex counts compared to the aforementioned algorithms. We chose to utilize SimGNN [30], a graph convolutional neural network which learns graph similarity metrics by leveraging comparisons between two graphs' overall structure and between their node-neighborhood structures.

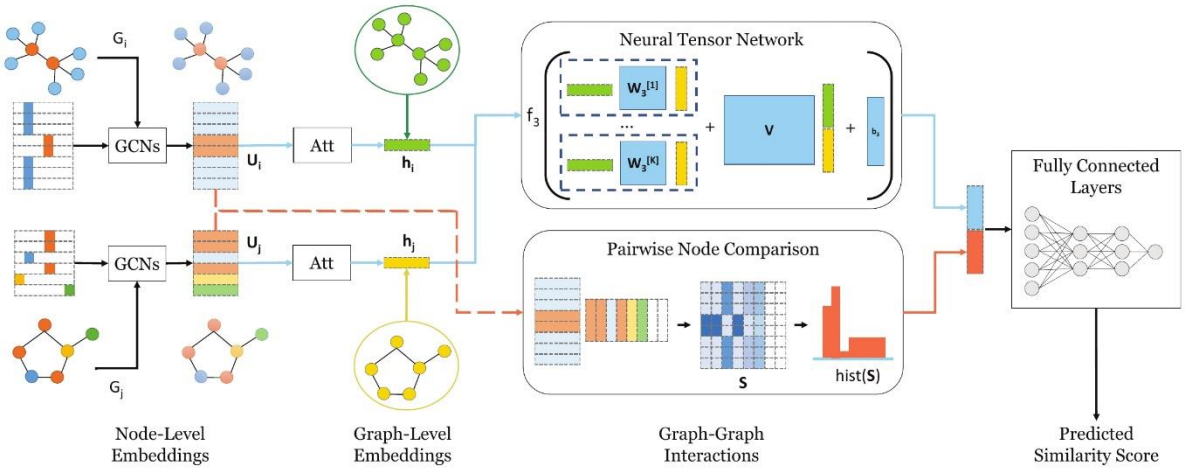

Figure A-1. Deep learning diagram [24].

The algorithm proceeds as follows: SimGNN takes as input encodings of the two input graphs whose similarity measure is desired. The algorithm first encodes the neighborhood of each node via an attention module to emphasize regions of each graph which are likely to impact the desired metric. Then in its graph-level module, the algorithm applies a graph convolution to compare the macroscopic structures of the input graphs. Separately, it convolves all pairs of node neighborhoods to detect localized nuances in the graph pair. Together, these modules produce a vector of abstract feature

scores that characterizes the similarity between the graphs, which is then reduced to a single similarity score: the desired metric.

Since the dynamics of our network are particularly complex, we are interested in the penultimate feature vector to give better resolution of topological similarity compared to the single output score. Taking after the originating authors of SimGNN [30], we train the network to compute GED. Since the graph disruptions in our simulations are relatively sparse, the true GED of our graph pairs is often the size of symmetric difference between disruptions from the ambient RTS, so this value is not enlightening. Yet, by focusing on the algorithm's penultimate feature vector rather than the single output score, we might obtain better resolution of the topological similarities that underpin the complex dynamics of our replicates.

Our method for obtaining these graph similarity vectors begins with processing the simulation data into format amenable to SimGNN. For each input, the PyTorch implementation of SimGNN we employ code from [30], publicly available on Github, that accepts a json file detailing the graphs: a dictionary with lists of edges and of node labels for each graph. To obtain these representations, we first model the intact RTS-96 network using Python's NetworkX package, which enables great visualizations. The nodes, edges, and attributes of the network are prescribed by the bus, line, transformer, and generator data proposed for the original system; buses and generators correspond to nodes while lines, transformers, and generators (again) correspond to edges. We process the list of simulated network failures then deprecate our graph accordingly. Throughout the disruption, we log simulation time so that we may use partially deprecated graphs as our data, rather than just the end-of-simulation replicate stages. In addition to animations portraying the simulated network disruptions over time, we produce images of the network status at each timestep; this proves to yield an improvement in interpretability over the tables specifying each failure event in isolation. We also display network attributes, like maximum bus voltages by end-of-simulation. Having visual expressions of the network's states aid in understanding what the SimGNN model is meant to notice as distinct between graphs in each pair. Moreover, we develop a sort of mean-state representation that allows many different replicates to be viewed in tandem, revealing topological features immediately characteristic to a cluster of deprecated networks.

With the network objects now reflecting the simulation results, we prepare them as input files for SimGNN. Pairs of the partially or fully deprecated graphs are exported to the necessary json files for input to SimGNN. Since these disruptions share a common supergraph (the intact network), we quickly compute an approximate GED for these pairs, using the symmetric difference of respective edge removals, to establish our testing and validation datasets.

In the initial training, each pair contains an intact network as one of the graphs. This ensures that our GED approximation is tight and should expedite learning. In one trial with SimGNN, we modify the architectural parameters (i.e. length of abstract feature vector, filter counts in the convolutional layer) to better account for the 3-way symmetry in the RTS-96 network. While we configure the neural network with varied learning parameters, we generally increase the epoch count compared to the implementation defaults. Unfortunately, these modifications do not seem to overcome shortcomings with our application.

While our implementation of SimGNN performs well on the sample training and testing datasets, this learning does not transfer to our data. The sample graphs have at most 20 nodes each, and only number 50 pairs; with as few as 5 epochs, the model learns GED effectively enough to perform suitably on the sample testing set. Regardless of using the sample training set of smaller graphs or our training set of deprecated RTS-96 networks, the model seems to learn very little knowledge that transfers to our validation set. At best, the model learns the average GED of our data and outputs similarities scores within a small range around this mean. At worst, the model misses the mean and outputs precise scores that are wholly inaccurate for our pairs.

We suspect the core impediment in application to our data is the large graph size paired with relatively few perturbations between graphs in the pairs. Indeed, the SimGNN authors acknowledged the lack of understanding of their model's performance on large graphs. The algorithm does not seem to notice the small differences in the input graph pairs; from the perspective of GED between large graphs, ours are very similar. The very characteristic of SimGNN that aims to eliminate bias against large graphs perhaps worsens this. The algorithm computes a normalized form of the GED that accounts for graph size in order to successful compare graphs of disparate sizes. However, when the graphs of interest are all large (and all large to a similar degree), the normalized GED scores are very small and lack much variance, making distinctions harder for the neural network to tease out in convolution. Still, the true GED values are dwarfed by the graph sizes (node and edge counts), and do not seem to improve performance on our data. Moving forward, modifications should be targeted to the model architecture which make use of characterizations of our data, such as the network symmetries and an outsized impact of node-neighborhood perturbations.

DISTRIBUTION

Email—Internal

Name	Org.	Sandia Email Address
Craig Lawton	08141	crlawto@sandia.gov
Raymond Byrne	08813	rhbyrne@sandia.gov
Technical Library	01977	sanddocs@sandia.gov

This page left blank

This page left blank

Sandia National Laboratories

Sandia National Laboratories is a multimission laboratory managed and operated by National Technology & Engineering Solutions of Sandia LLC, a wholly owned subsidiary of Honeywell International Inc. for the U.S. Department of Energy's National Nuclear Security Administration under contract DE-NA0003525.